Shape memory alloys applied to improve rotor-bearing system dynamics - an experimental investigation

Enemark, Søren; Santos, Ilmar; Savi, Marcelo A.

Published in:
Proceedings of the 17th International Symposium on Dynamic Problems of Mechanics

Publication date:
2015

Document Version
Publisher's PDF, also known as Version of record

DINAME 2015 - Proceedings of the XVII International Symposium on Dynamic Problems of Mechanics
V. Steffen, Jr; D.A. Rade; W.M. Bessa (Editors), ABCM, Natal, RN, Brazil, February 22-27, 2015

Shape memory alloys applied to improve rotor-bearing system dynamics – an experimental investigation

Søren Enemark[1*], Ilmar F. Santos[1], and Marcelo A. Savi[2]

[*] Corresponding author, soene@mek.dtu.dk.

[1] Technical University of Denmark, Department of Mechanical Engineering, DK-2800 Kgs. Lyngby, Denmark

[2] Universidade Federal do Rio de Janeiro, COPPE - Department of Mechanical Engineering, 21.941.972 - Rio de Janeiro - RJ - Brazil, P.O. Box 68.503

Abstract: Rotor-bearing systems have critical speeds and to pass through them is an ongoing challenge in the field of mechanical engineering. The incorporation of shape memory alloys in rotating systems has an increasing importance to improve system performance and to avoid potential damaging situations when passing through critical speeds. In this work, the feasibility of applying shape memory alloys to a rotating system is experimentally investigated. Shape memory alloys can change their stiffness with temperature variations and thus they may change system dynamics. Shape memory alloys also exhibit hysteretic stress-strain relations which may be utilized for damping purposes. These ideas are tested in this study on a dedicated test-rig, consisting of a rigid shaft and disc held vertically by passive magnetic bearings, where the damping is low. The bearing housings is flexibly supported by shape memory alloy helical springs, and because of high dynamic coupling between shaft and bearing housing, the shape memory alloy springs are able to reduce vibration in the shaft. The shape memory alloy springs are characterized by force-displacement tests in different temperatures. Transients of step perturbations and mass imbalance responses of the rotor-bearing system at different temperatures and excitation frequencies are carried out to determine the dynamic behaviour of the system. The behaviour and the performance in terms of vibration reduction and system adaptability are compared against a benchmark configuration comprised by the same system having steel springs instead of shape memory alloy springs. The experimental results clearly show that the stiffness changes and hysteretic behaviour of the shape memory alloys springs alter system dynamics both in terms of critical speeds and mode shapes. Vibration peaks could be reduced up to 47 % during ramp-up tests compared to the system configuration with steel springs and the two first critical frequencies could be altered up to 7 % by temperature changes.

Keywords: Shape memory alloys, rotor-bearing systems, dynamics, experiments, hysteretic damping

INTRODUCTION

Shape memory alloys (SMAs) show a variety of remarkable characteristics, which is why they have been widely investigated in the last decades. They have been used in civil engineering for seismic isolation (Janke et al., 2005) and for aerospace applications for customising inlet geometries of propulsion systems (Lagoudas and Hartl, 2007) for example. In rotating systems, the purpose of bearings is typically three-parted: to have low friction so energy losses are reduced, to reduce vibrations of the shaft and to have sufficient load capacity. In some bearings, e.g. air bearings and passive magnetic bearings, the friction is low compared to conventional bearings, but the damping capabilities are limited. Incorporation of SMAs might be able to change this.

Liang and Rogers (1993) highlighted strategies of using SMAs in vibration attenuation: (1) SMAs have different stiffness in low and high temperature because of transformation between martensitic and austenitic crystallographic phases, and the stiffness change can be used to alter system resonance frequencies; (2) the transformation between martensite and austenite may induce high levels of strain (up to 8 %), and therefore SMAs could be used as an actuator; (3) furthermore the transformations (either induced by temperature or stress variations) exhibit large amounts of hysteresis, which could be used for damping purposes; (4) finally since the martensitic phase exists in different variants, similar hysteretic characteristics are found when the material undergoes martensitic reorientations as a consequence of stress variations.

The idea of incorporating SMAs in rotor-bearing systems was first suggested by Nagaya et al. (1987), who proposed a stiffening changing device for the bearing housings based on an SMA actuator. By changing the stiffness, the system resonance frequencies were altered, and by changing between the two system configurations the critical speed could be avoided during run-up or run-down scenarios. The investigations were primarily theoretical, but some experimental results were also presented, and the idea was found feasible.

Nie and Yan (2000) showed similar experimental results and highlighted that the change in stiffness must be abrupt in order to avoid exciting eigenmodes with low damping, which potentially could be equally undesirable as passing through a critical speed. An abrupt stiffness change is almost impossible and therefore appropriate damping is also required. Aravindhan and Gupta (2010) investigated the simultaneous use of SMA stiffness switching elements and magneto-

rheological (MR) dampers in rotor vibration control. The switching start point in time and switching duration times during a run-up were investigated along with different amounts of MR damping. They concluded that stiffness switching (with realistic switching durations) does not reduce the level of vibration when passing through a critical speed as long as the MR damping is sufficiently high. MR damping is hysteretic and therefore it is comparable to the hysteretic damping of the SMA phase transformations.

Żak et al. (2003) and Inman et al. (2006) described a bearing housing design consisting of a composite sleeve-ring with SMA strips attached to control eigenfrequencies and mode shapes of a rotor-bearing system. They found out that simple supports (as opposed to clamped boundary conditions) and highly compliant sleeve-ring give highest adaptability. In the latest configuration additional SMA strips were inserted opposite to the others to perform 'antagonistic action', i.e. when cooling one SMA element the opposite element is heated in order to improve the actuator bandwidth (Inman et al., 2006). The same group, Lees et al. (2007), also suggested to use SMA wires as a preload mechanism of an elastomer bearing, whose restoring forces were non-linear so that the bearing stiffness depended on the preload and therefore the SMA temperature. The findings of this group were summarised by Cartmell et al. (2012).

He et al. (2007a,b) also investigated the subject theoretically and experimentally on a shaft with a disc supported at both ends; at one end the bearing housing was supported by SMA springs. An algorithm was proposed to determine the optimal stiffness (and thereby temperature) of the SMA depending on the rotational frequency in terms of vibration attenuation of the disc. Gupta et al. (2009) made a similar theoretical and experimental analysis on a rotor with disc supported by SMA springs in both ends. Also Borges et al. (2013) made experiments on a similar test-rig, where the SMA temperature (and therefore stiffness) was actively controlled by a fuzzy controller using the acceleration of the disc as input.

To the authors' knowledge the third and fourth strategies proposed by Liang and Rogers (1993), i.e. using the hysteretic effects in SMAs to dissipate energy, has not yet been experimentally employed in rotor-bearing systems. Aguiar et al. (2013) investigated generic 1 and 2 degrees-of-freedom systems with SMA support to illustrate the capabilities of SMAs in terms of hysteretic damping and temperature dependent stiffness. Another experimental study was made by Enemark et al. (2014) with the same aim on a 1 degree-of-freedom system, where also the transient behaviour and moving equilibria were investigated on SMA springs exhibiting pseudoelasticity and shape memory effect. In both studies it was highlighted that the hysteretic properties vanish in high temperature, which establish a trade off between conducive stiffness changes and loss of damping.

In this work, both stiffness changes caused by temperature variations and the hysteretic damping characteristics of pseudoelastic SMA springs are exploited in a dedicated rotor-bearing test-rig having passive magnetic bearings. The bearing housings are flexibly supported by SMA helical springs. By having high coupling between rotor and bearing housing dynamics, it is possible to dissipate vibration energy through the bearing housings. The goal is to enhance the performance of the system dynamics primarily in terms of vibration reduction of the rotor and system adaptability, associated with the system being able to change dynamic characteristics as a consequence of the SMA environment temperature. A benchmark system configuration is used, where steel springs having similar linear stiffness substitute the SMA springs in order to evaluate the performance change. This work is original in the sense that both temperature induced stiffness changes and hysteretic damping capabilities are utilized. Cold, hot and intermediate SMA temperature states are investigated. Because the passive magnetic bearings and the SMAs have similar stiffnesses, the rotor-bearing interaction become an important design aspect. In the investigations found in the literature, both theoretical and experimental, the rotor-bearing interactions have been considered rigid.

EXPERIMENTAL PROCEDURES

The experimental rotor-bearing test-rig designed for this work may be seen in Fig. 1 (picture and schematics) together with the reference system XYZ. The rotor-bearing system consists of a vertical rigid shaft, and at its upper end a disc is attached. The disc facilitates adjustable mass imbalance. The bottom of the shaft is connected to a DC motor through a flexible coupling, and thereby the shaft and disc are able to tilt around the X and Y axes. The shaft is supported by two passive magnetic bearings having positive horizontal stiffness. The magnetic bearing housings are themselves flexibly supported by means of clamped-clamped steel beams: The upper bearing housing is connected to the lower bearing housing by beams only compliant in the Y direction; The lower bearing housing is connected to the ground by beams only compliant in the X direction. This means that the two bearings move synchronously in the X direction and that the upper bearing only moves in the Y direction relative to the lower bearing. The upper bearing could be supported additionally by either SMA helical springs or steel helical springs in both horizontal directions in both sides (four springs in total) defining different system configurations. A system involving two heat guns, two thermocouples and a heat chamber for each of the four springs facilitates control of the SMA (or steel) spring environment temperature. Designating the four spring positions North (N), East (E), South (S) and West (W), the heat chamber temperatures are controlled in pairs; N and W together and S and E together.

Rotor tilt (in X and Y), rotor angular position (around Z), upper bearing housing acceleration (in X and Y) and SMA springs/steel spring forces (in X and Y) were measured. However, because of inertia effects in the force decoupling

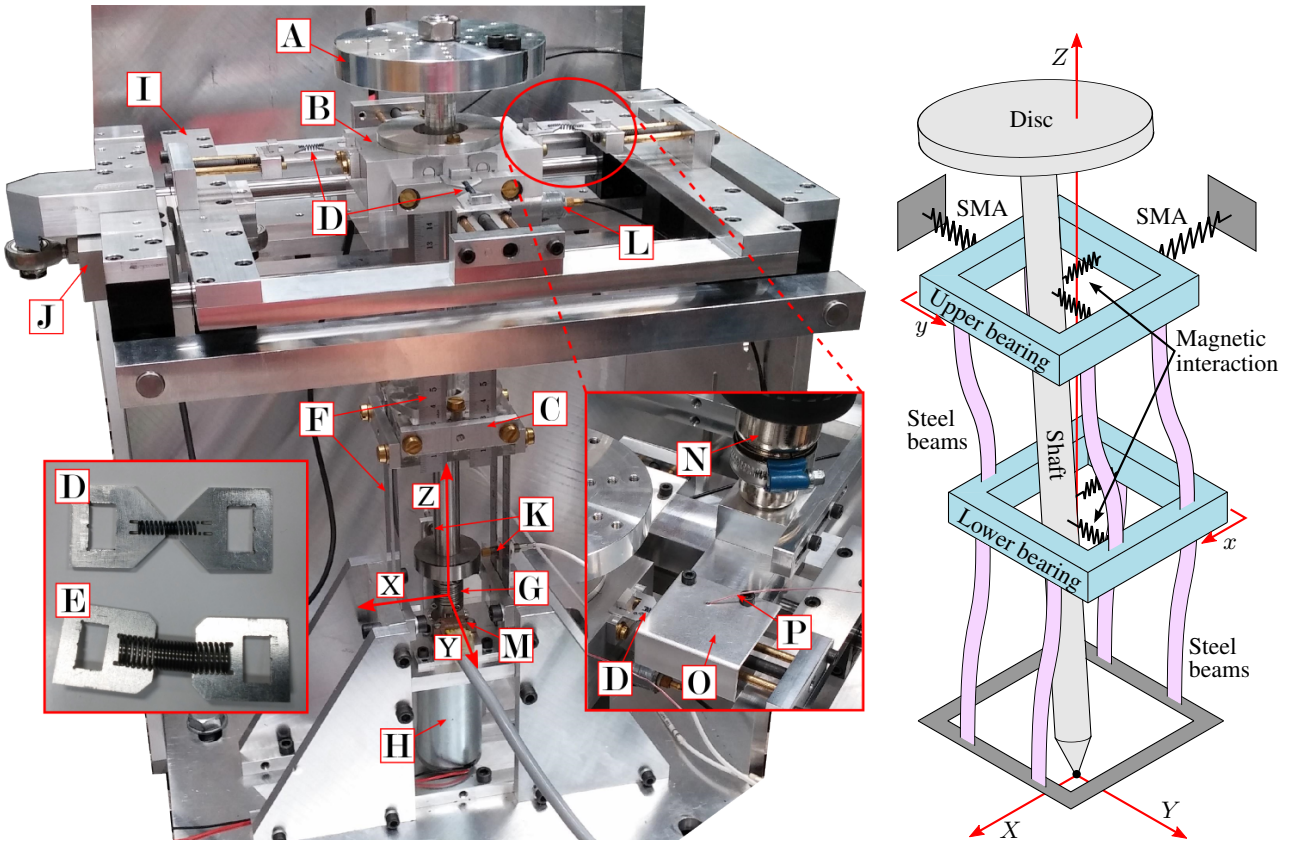

(a) (b)

Figure 1: Picture (a) and schematics (b) of smart rotor-bearing test-rig. (a) show the disc on the rigid shaft (A), upper (B) and lower (C) passive magnetic bearings, SMA (D) or steel (E) springs, flexible beams (F) for supporting the bearing housings, a flexible coupling (G) at the shaft end, a DC motor (H), a structure (I) for decoupling SMA or steel spring forces, one of two force transducers (J) for measuring SMA or steel spring forces, two proximitor sensors (K) for measuring shaft tilt, one of two accelerometers (L) for measuring bearing motion, an encoder (M) for measuring rotor angular position and velocity, heat gun nozzle (N) and heat chamber (O) for temperature control using measurements from thermocouples (P) in heat chamber. In (b) the light grey disc and shaft are supported by the blue lower and upper passive magnetic bearings. The bearings are supported by the purple flexible beams. Upper bearing housing is also connected through SMA or steel springs to a fixed part.

structure (Fig. 1(a) part I), the force measurements were not representative for the SMA forces. Therefore, the force measurements have been omitted in this work.

Characterization of the SMA helical springs consists of force-displacement tests at different environment temperatures. Similar experiments were performed on the steel springs. The experimental characterization of the rotor-bearing system in different configurations (spring type and environment temperature) comprises:

1. Transient responses as consequence of step perturbations on the rotor disc at different spring environment temperatures. This gives information on free vibration period and damping capabilities.
2. Rotor mass imbalance responses at different excitation frequencies and spring environment temperatures resulting in experimental steady state imbalance response relations.
3. Rotor mass imbalance ramp-up tests in different spring environment temperatures highlighting vibration peaks and transient behaviour.
4. System applications showing the potential of introducing control of the SMA environment temperature to facilitate stiffness switching strategies.

Performance of the system in its different configurations is evaluated in terms of level of vibration reduction (peak response), dissipation of energy (duration of transient vibrations) of the rotor and also system adaptability.

RESULTS & DISCUSSION

In this section the experimental results are presented and analysed.

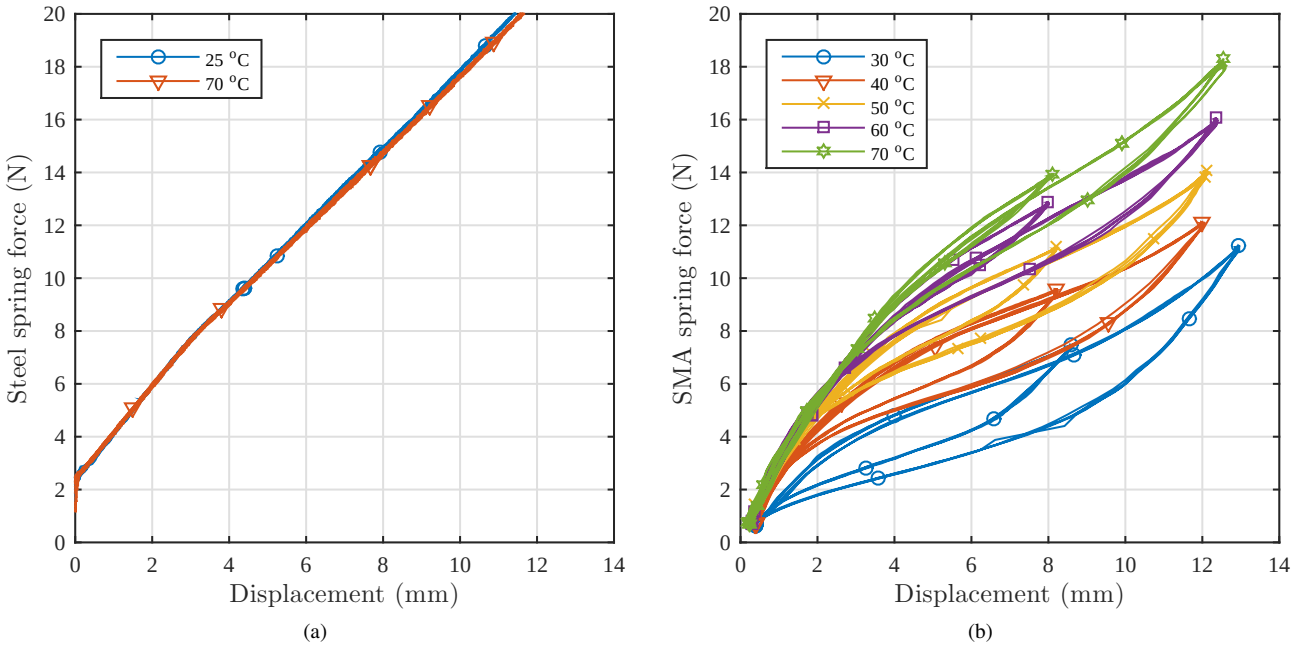

Figure 2: Force-displacement tests of (b) steel spring and (a) SMA helical spring in different temperatures.

Spring characterizations

Force-displacement relationships of the SMA springs and steel springs may be seen in Fig. 2. The results show that the steel spring is a clear linear force-displacement relationship for displacements above approximately 3.5 mm (relative to the relaxed state), where there is a slight bend. The environment temperature does not affect the stiffness significantly; the steel spring stiffness is 1.46 N/mm at 25 °C and 1.43 N/mm at 70 °C resulting in a relative difference of 2 %. Lastly, the steel spring does not show any hysteretic properties.

The force-displacement relationship of the SMA spring (Fig. 2(b)) is more complicated; the results show clearly pseudoelastic properties involving significant hysteresis, changing stiffness and a strong thermomechanical coupling. The SMA spring was exposed to two excitation levels of approximately 8 mm and 12 mm for every temperature. The results consist of five successive loading cycles for each excitation level and temperature. At 30 °C the stiffness varies between approximately 0.4 N/mm to 2.0 N/mm depending on the level and direction of load. The stiffness is calculated using the tangential inclination of the curve. At 70 °C the stiffness is generally higher, namely between approximately 0.8 N/mm and 3.7 N/mm. The initial stiffness (reflecting the austenitic state) is 1.6 N/mm at 30 °C, whereas it is approximately 3.7 N/mm at all other temperatures. This could indicate that the spring is not in a fully austenitic state in the relaxed state at 30 °C. After the turning points in the large loop (reflecting a mixture of austenite and martensite) the stiffness is almost independent of the temperature; it is approximately 1.7 N/mm. The area of the hysteresis loop is largest at room temperature. However, it is still present at high temperatures, meaning that hysteretic damping should be available also in these conditions.

The steel and SMA springs have similar stiffnesses meaning that when employed in the rotor-bearing test-rig, the responses should be comparable. If the stiffnesses had been significantly different, the system mode shapes would change, making it impossible to compare peak amplitudes. When employed in the test-rig the pretension levels were approximately 5 mm for the steel springs and 3 mm for the SMA springs.

System transient dynamics

After inserting either four SMA or steel springs in the test-rig highlighted in Fig. 1, transient responses of the rotor were captured, after releasing the rotor at an initial tilt angle. Only the lowest critical speed is excited this way. The test was carried out three times for different SMA environment temperatures. A typical response is shown in Fig. 3(a) highlighting vibration period (detected from zero crossing) and the vibration envelope.

Rotor vibration envelopes are shown in Fig. 3(b) for different system configurations. Only the results of the X direction are shown. In this coordinate system, where the vertical axis is logarithmic, viscous damping would result in a straight line having a slope proportional to the damping factor. The slope of envelope for the steel configuration is close to linear indicating viscous damping. The lines of the SMA configurations are not linear but close to piecewise linear having a bend at approximately 2 seconds. In the initial seconds, where the vibration amplitudes are large, the slopes are higher (in absolute sense) showing high level of damping due to the hysteretic phase transformations. After $t = 2$

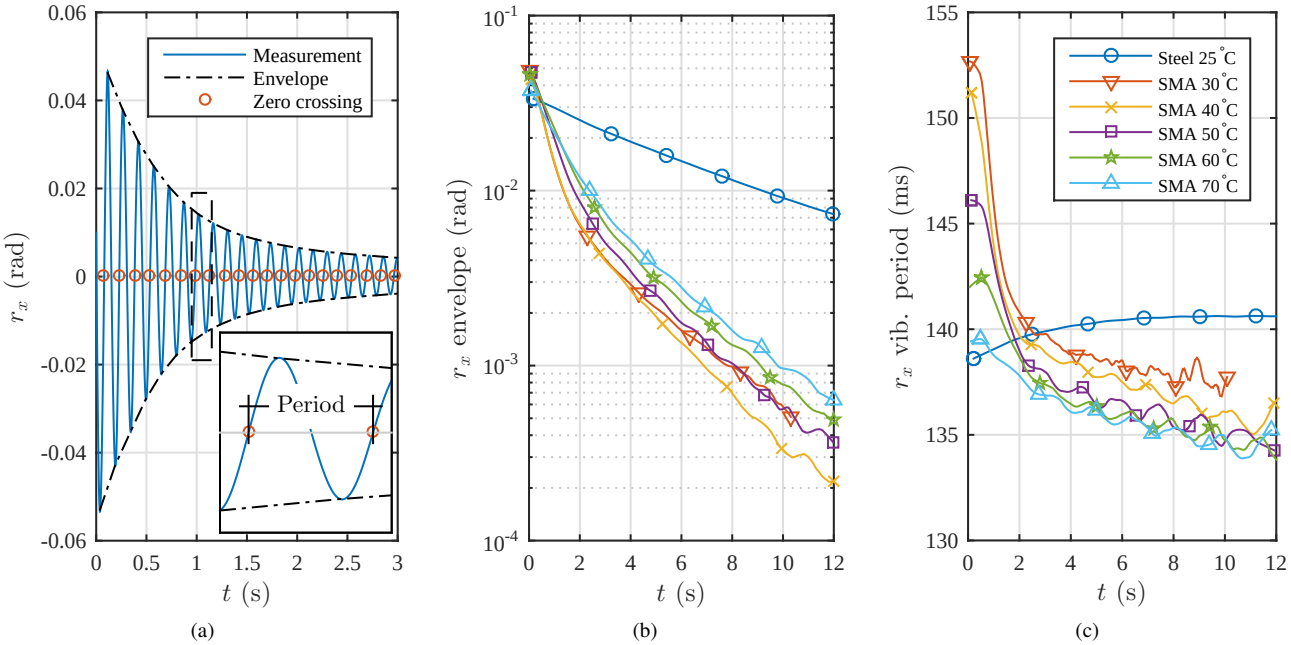

Figure 3: Transient behaviour of rotor. (a) Example of transient response highlighting the evolution of the vibration envelope and vibration period. Evolution of (b) vibration envelope and (c) vibration period over time at different temperatures for the SMA spring and for the steel spring in room temperature.

s, the slopes decrease because the hysteretic phase transformations does not take place at low amplitudes. Based on the slopes of the lines the damping is much higher in the SMA systems in general compared to the steel configuration. The initial slope of the 30 °C and 70 °C SMA configurations are 8 and 4 times higher than for the steel system respectively. The low amplitude slopes are almost independent of the SMA temperature, and they are 2.5 times higher than the steel configuration slope.

The vibration period as function of time is highlighted in Fig. 3(c). The steel configuration shows an almost constant vibration period of approximately 140 ms (7.1 Hz). On the other hand, the vibration period of the SMA system configurations changes drastically in the initial seconds, where the vibration amplitudes are high. The decrease in vibration period is largest in the lower temperature configurations. Moreover, the vibration period is generally slightly lower in high temperatures. This means that the SMA exhibits lower stiffness at high amplitudes and low temperatures, which is in agreement with the force-displacement tests presented in the former section. After a couple of seconds the vibration period only slowly decreases indicating less hysteretic behaviour. This means that the system critical speeds depend both on the excitation level and the temperature in the SMA configuration making the system response nonlinear. The results of vibration envelope and period in the Y direction are similar to the results of the X direction and are not shown here.

Imbalance responses

By exciting the system using mass imbalance at the rotor disc at different constant frequencies, steady state responses were determined. These are shown in Fig. 4 for both the rotor (r_x, r_y) and the upper bearing housing (b_x, b_y). The lower bearing has coordinates (b_x, 0). The plot shows the amplitude of the synchronous component of the response obtained over a 5 second sample. Generally, measurements were taken with intervals of 0.5 Hz in rotor angular velocity and with intervals of 0.1 Hz around resonances. The results comprises up and down frequency sweeps to check for consistency.

The system is a 4 degrees-of-freedom system (in the frequency range of interest), and therefore 4 critical speed are present in Fig. 4. Movements in the X and Y planes are almost uncoupled, meaning that the first and third critical speeds are only detected in r_x and b_x and the second and fourth critical speeds only in r_y and b_y. The first and second modes consist of in-phase motion of rotor and bearing, whereas the third and fourth modes comprise counter-phase motion. In some conditions the damping capabilities are so low that rotor-bearing impacts occur during resonance. This is seen in all resonances for the steel system and in the first and second resonance of the 70 °C SMA system. The resonance peaks using the SMA system configurations are non-symmetric indicating nonlinearities in the system. This means that the critical speeds depend on the excitation level.

Frequencies and vibration amplitudes of the rotor in the four critical speeds are shown in Tab. 1. The amplitude in first and second modes are an order of magnitude larger than in third and fourth. Also the frequency of the third and fourth modes are more sensitive to the SMA temperature. It should be noticed that the resonance amplitude of the fourth

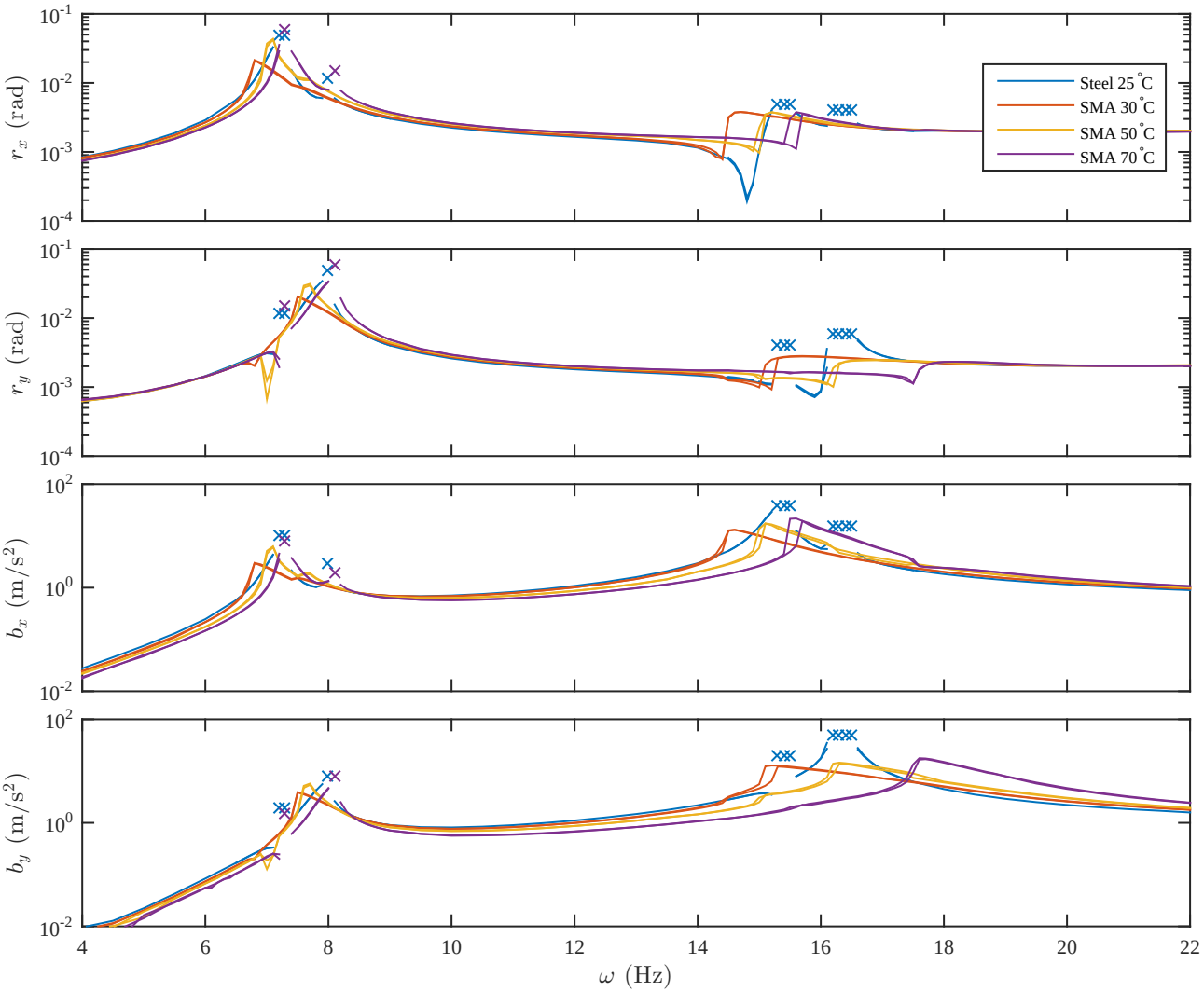

Figure 4: Amplitude of steady state imbalance responses. Crosses ($\times$) indicate conditions with rotor-bearing impacts caused by insufficient damping.

mode actually decreases with increasing SMA temperature even though the level of hysteretic damping decreases with increasing temperature. This clearly indicates that not only the level of damping but also the construction of mode shapes is an important design strategy when using SMAs in rotor vibration control of this system. A further reduction of the vibration amplitude in first and second modes could be accomplished by having better damping properties of the SMAs. However, in case of too high damping, significant changes towards weak dynamic coupling between rotor and bearing housing would result in an increase of rotor vibrations and an inefficient use of the SMA elements. Efficient use of SMA springs or other damping mechanisms in connection to flexible suspension of bearing housing requires strong coupling between the rotor and bearing housing movements.

At some critical speeds there are discrepancies between the up and down sweeps when using the SMA configurations. This is clear at the third critical speed using the 70 °C SMA configuration for example. This means that there are co-existing steady states, which is typical for systems with nonlinear stiffness and low level of damping. However in this system the damping is relatively high. The co-existing states are caused by the latent heat of the phase transformations which means that the actual SMA temperature could be higher than the environment giving the SMA other stiffness and damping characteristics. Approaching the critical speed from the left (sweep up), where the amplitudes are small, the latent heat effect would not be as predominant as when approaching from the right (sweep down), where the amplitudes are higher. This means that the actual SMA temperature is higher when approaching from the right giving two different system conditions. It would not be possible to jump between the two co-existing states in a chaotic manner because this would require fast temperature changes. It also means that the states are actually not co-existing if the SMA temperature is considered as a state variable. The discrepancies could have been avoided by having better convective conditions (increasing forced convection or changing environment medium).

Ramp-up tests are shown in Fig. 5 for the bearing and rotor in the X direction. The results in the Y direction are similar. The vibration envelopes are based on three tests in each system configuration. The peak vibration amplitudes

Table 1: Frequency and amplitude of the rotor at the four critical speeds using different system configurations (type of spring and temperature). A dash (–) indicates that the amplitude was so high that rotor-bearing impacts occurred during testing.

r_x	Frequency (Hz)		Amplitude (10^{-3} rad)	
Conf. \ Crit. sp.	1st	3rd	1st	3rd
Steel 25 °C	≈ 7.2	≈ 15.4	–	–
SMA 30 °C	6.8	14.7	21	3.8
SMA 50 °C	7.1	15.2	43	3.8
SMA 70 °C	≈ 7.3	15.6	–	3.8

r_y	Frequency (Hz)		Amplitude (10^{-3} rad)	
Conf. \ Crit. sp.	2nd	4th	2nd	4th
Steel 25 °C	≈ 8.0	≈ 16.3	–	–
SMA 30 °C	7.5	15.7	20	2.8
SMA 50 °C	7.7	16.9	30	2.5
SMA 70 °C	≈ 8.1	18.2	–	2.3

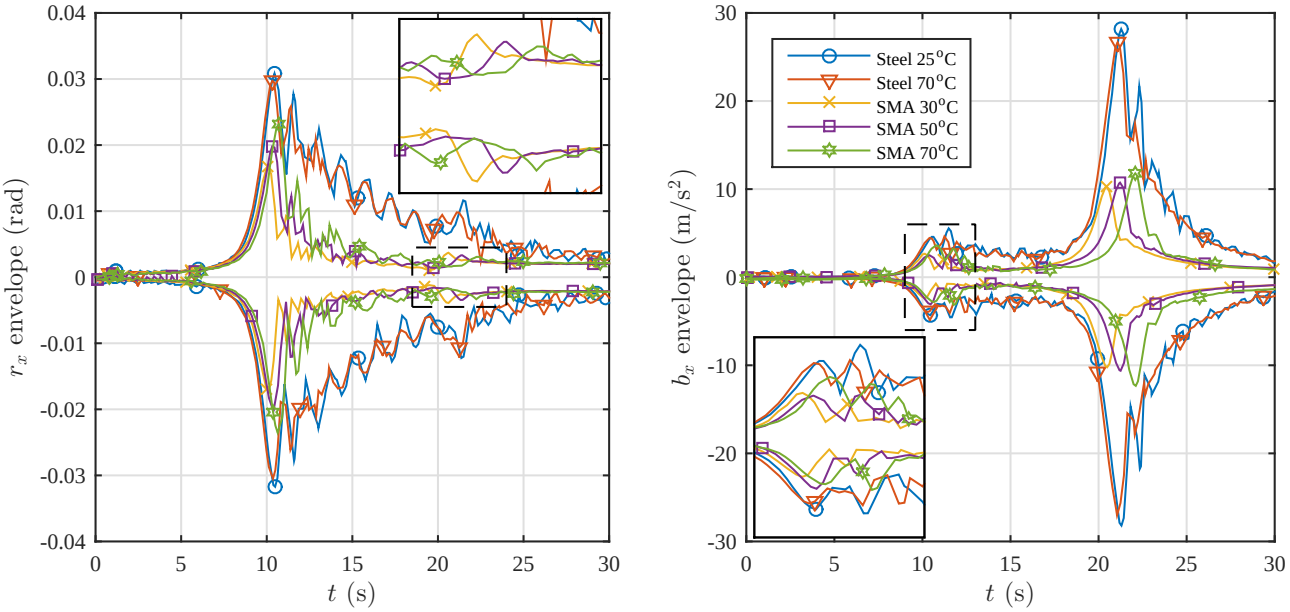

Figure 5: Envelope of rotor mass imbalance response in X direction of ramp-up from 0 Hz to 25 Hz with a constant angular acceleration of 0.75 Hz/s ($t = 0$ s corresponds to 0 Hz and $t = 30$ s corresponds to 22.5 Hz).

of the rotor during ramp-up are highlighted in Tab. 2 for both the X and Y directions. There are two steel spring configurations, namely 25 °C and 70 °C. The ramp-up tests show almost identical results for the two configurations; the slight discrepancies are due to the fact that the 70 °C steel spring is slightly less stiff. The peak amplitude and transients are similar in the two configurations indicating same level of damping.

For the SMA configurations the peak amplitudes are considerably lower and the duration of the transients are considerably shorter because of higher damping. The duration of the transients are similar among the SMA configurations indicating similar levels of damping. However, the peak amplitude of the rotor associated with the first excited mode is lowest at low temperatures, which indicates higher level of damping but also a more effective mode shape in terms of rotor-bearing coupling. It is opposite for the bearing. However in the third mode (second peak at $t = 21$ s) the peak amplitude of the rotor is lower at higher temperatures. Again it is opposite for the bearing. This indicates that the mode shapes are more effective in terms of coupling from the rotor point of view in high temperatures in the third and fourth critical speeds, where the they counteract the lower level of hysteretic damping. These observations are in agreement with the conclusions drawn above based on the steady state responses.

Application cases

In this section five different cases are presented highlighting the opportunities of using SMAs to control rotor vibrations. The first three cases are associated with Fig. 6. The first case, highlighted in Fig. 6(a), shows the vibrations in r_x due to rotor mass imbalance at 6.8 Hz at 30 °C. This is exactly at the first critical speed, cf. Tab. 1. By changing the SMA environment temperature to 70 °C, the vibrations in r_x are reduced by 78 %, because the critical speed moves away from the excitation frequency. Figure 6(b) shows the vibrations in r_y at 8.0 Hz, which is slightly below the second critical speed of 8.1 Hz. By reducing the temperature the critical speed crosses the excitation frequency (it is possible to see a

Table 2: Peak vibration amplitude of the rotor during ramp-up crossing the four critical speeds using different system configurations (type of spring and temperature).

r_x	Amplitude (10^{-3} rad)		r_y	Amplitude (10^{-3} rad)	
Conf. \ Crit. sp.	1st	3rd	Conf. \ Crit. sp.	2nd	4th
Steel 25 °C	32	12	Steel 25 °C	32	14
Steel 70 °C	30	11	Steel 70 °C	32	13
SMA 30 °C	17	4	SMA 30 °C	19	3
SMA 50 °C	20	3	SMA 50 °C	24	3
SMA 70 °C	24	3	SMA 70 °C	29	4

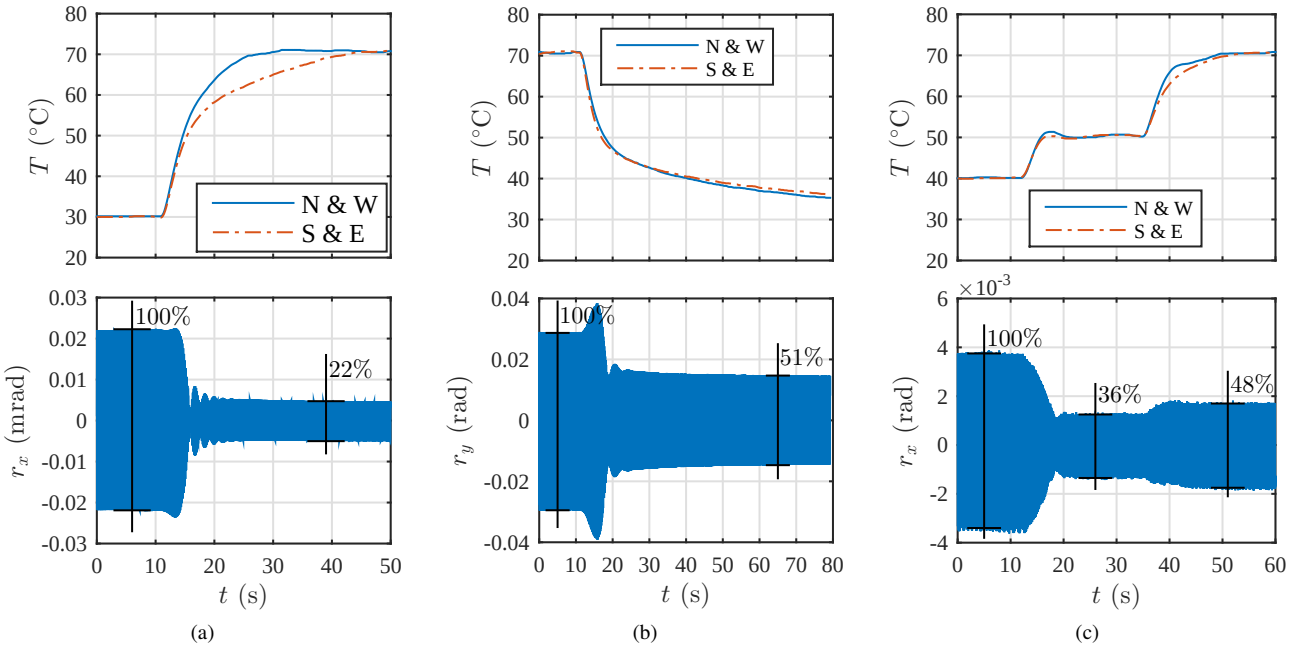

Figure 6: Changes in rotor imbalance response as consequence of heat chamber temperature variations. The rotational frequencies are (a) 6.8 Hz, (b) 8.0 Hz and (c) 15 Hz.

vibration peak at $t = 15$ s) and then moves away resulting in a vibration reduction of 49 %. It ia also possible to utilize anti-resonances as shown in Fig. 6(c). Here the excitation frequency is 15 Hz and the SMA environment temperature is 40 °C. By changing the temperature to 50 °C the rotor enters an anti-resonance condition, cf. Fig. 4, and the vibrations are reduced by 64 %. The anti-resonance frequency moves away from the excitation frequency when the temperature is increased further to 70 °C resulting in larger vibrations.

With the goal of reducing vibrations in the rotor during ramp-up it is beneficial to keep a low temperature when crossing the first and second critical frequencies and a high temperature when crossing the third and fourth critical frequencies, cf. Fig. 5(a). Therefore a test was performed where the environment temperature was altered after crossing the first and second critical frequency during a ramp-up. The results are shown in Fig. 7(a), and they are compared to the 30 °C and 70 °C static temperature configurations. The vibration envelope of the dynamic temperature case follows the 30 °C configuration at the first critical speed and the 70 °C configuration at the third critical speed, and thereby the vibrations are minimized in the whole range.

In this system, the highest rotor vibration peaks are associated with the first and second critical speeds, and they should therefore be in focus in terms of vibration attenuation during ramp-up. The usual approach described in the literature for vibration attenuation during ramp-up using SMAs involves changing the resonance frequency from a higher value (high SMA temperature) than the excitation frequency to a lower value (low SMA temperature) while slowly ramping up, cf. Nagaya et al. (1987); Nie and Yan (2000); He et al. (2007a,b); Gupta et al. (2009); Aravindhan and Gupta (2010). The idea is that the critical speed is crossed at a faster rate compared to a simple ramp-up in constant temperature conditions, meaning that transients have shorter time to build up. An example of this strategy is shown in Fig. 7(b). The first critical speed is crossed while the temperature decreases from 50 °C towards 30 °C. However, compared to the ramp-up in 30 °C, the vibration peak is larger, as may be seen in the zoomed in section to the left. In the first and second critical speeds

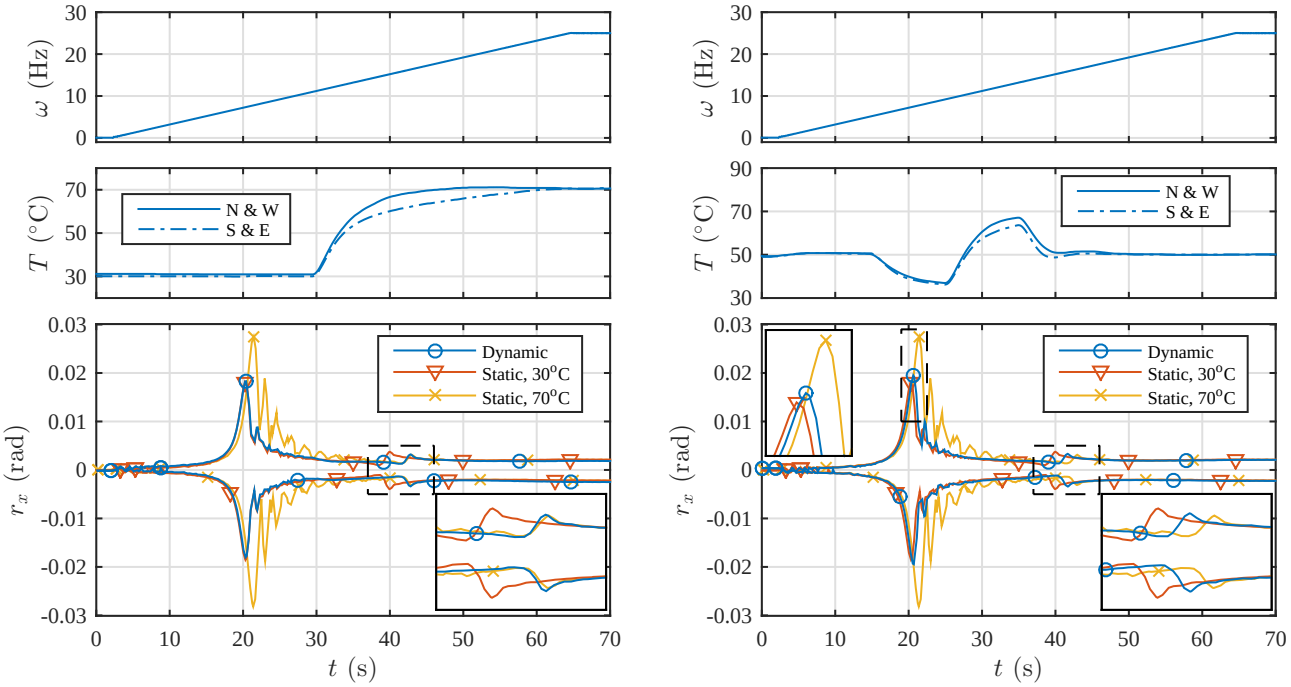

Figure 7: Transient responses in r_x of ramp-up tests using either constant temperature at 30 °C or 70 °C or time varying (dynamic) temperature.

the coupling of rotor-bearing housing movements and the damping characteristics are highest in lowest temperature (30 °C). Therefore it is not desirable to let the actual crossing happen at an intermediate temperature, which is necessary in the switching strategy, even though the crossing would happen slightly faster. If however the temperature switching could happen faster, it could have been beneficial, cf. Aravindhan and Gupta (2010), because transients then would have had a shorter time span to build up. Finally, the frequencies of the first and the second critical speeds are very close in this system. This means that stiffness switching scheduling would require the system to switch temperature rapidly several times, which is infeasible in this system.

CONCLUSION

In this work the effect of using SMAs to control vibrations of an experimental rotor-bearing test-rig was investigated and the results were compared to a system configuration using steel springs instead of SMA springs. By using springs with similar stiffness the rotor-bearing system responses were comparable. The SMA springs exhibited high thermomechanical coupling, strong hysteresis and changing stiffness (from 0.4 N/mm to 3.7 N/mm). In a temperature range from 30 °C to 70 °C the hysteresis was most significant in the lower temperatures. The steel spring was linear and its stiffness (1.43 N/mm to 1.46 N/mm) only changed 2 % depending on its temperature.

Transient responses of the rotor-bearing system excited in its first critical speed showed that the damping capabilities of the SMAs due to the hysteresis were highest at high vibration amplitudes and low temperatures. The frequency of the free vibrations also depended on the vibration amplitudes. Compared to the steel spring system configuration, the damping of the SMA system was 2.5 to 8 times higher (in terms of damping factor) again depending on amplitude and temperature.

Steady state rotor mass imbalance responses showed that the vibration amplitude of the rotor at the first and second critical speeds were smallest when having a low SMA temperature. At high SMA temperatures and with the steel springs, the vibration amplitudes were so high that rotor-bearing impacts occurred because of low damping. In the third critical speed the vibration amplitude was independent on SMA temperature, whereas it was smallest for highest temperatures at the fourth critical speed. The first two (and crucial) critical frequencies could be moved 7 % by varying the SMA environment temperature, which defined the system adaptability.

During a ramp-up test the peak vibration amplitude of the rotor (associated with the first and second critical speeds) was reduced by 9 % to 47 % when using SMA springs in high and low temperatures respectively instead of using steel springs. These results showed that changing the SMA stiffness did not only change the critical frequencies but also the mode shapes. Therefore, the vibration level of the rotor did not only depend on the hysteretic damping of the SMA (which was largest at low temperatures) but also the mode shapes, which define the relation between the vibration level of the

rotor and bearing housings. This also means that control of this rotor-bearing system using SMAs would require a holistic design approach not only focused on the SMA component (the actuator) but also on the system components and their interaction. Transient analyses during ramp-up tests showed that it was best in terms of rotor vibration attenuation to pass the first two critical speeds using an SMA temperature of 30 °C and the third and fourth critical speeds using 70 °C. In the literature it has been proposed to switch the stiffness from high to low right before passing a critical speed in order to simply avoid it. However, this approach was not feasible for this system because the stiffness switching was not instantaneous but slow. This means that when stiffness switching scheduling was used, the critical speed was crossed in almost the same rate as when the temperature was held constant. Additionally, the dynamic coupling between rotor and bearing housing (defining the mode shapes) and the damping characteristics were highest at the lowest temperature associated with low SMA stiffness.

ACKNOWLEDGEMENTS

We thank the Danish Ministry of Science, Innovation and Higher Education for the support to the FTP Research project 12-127502 and the Brazilian National Council for Scientific and Technological Development (CNPq) for the support to project 400364/2012-3 of the program Science Without Borders. We also acknowledge the support of the Brazilian Research Agencies CNPq, CAPES and FAPERJ and through the INCT-EIE (National Institute of Science and Technology – Smart Structures in Engineering) the CNPq and FAPEMIG.

REFERENCES

Aguiar, R.A.A., Savi, M.A. and Pacheco, P.M.C.L., 2013, Experimental investigation of vibration reduction using shape memory alloys, Journal of Intelligent Material Systems and Structures, Vol. 24, No. 2, pp. 247–261.

Aravindhan, T.S. and Gupta, K., 2010, Multiple smart material applications using SMA and MR fluid damper for rotor vibration control, Proceedings of the ASME Turbo Expo, Vol. 6, pp. 299–308.

Borges, J.M., Silva, A.A., de Araújo, C.J., Fernandes, E.d.M., Pimentel, R.L. and Santiago, A.A., 2013, Rotor-bearing vibration control system based on fuzzy controller and smart actuators, International Journal of Multiphysics, Vol. 7, No. 3, pp. 197–205.

Cartmell, M.P., Żak, A.J. and Ganilova, O.A., 2012, Applications for shape memory alloys in structural and machine dynamics, in J. Warminski, S. Lenci, M.P. Cartmell, G. Rega and M. Wiercigroch (Eds.) Nonlinear Dynamic Phenomena in Mechanics, Springer Netherlands, Vol. 181 of *Solid Mechanics and Its Applications*, pp. 115–158.

Enemark, S., Savi, M.A. and Santos, I.F., 2014, Experimental analyses of dynamical systems involving shape memory alloys, Smart Structures and Systems, in press.

Gupta, K., Darpe, A.K., Kumar, B., Bhatia, A., Ahmed, S.M., Aravindhan, T.S. and Nakra, B.C., 2009, Resonance control of rotor using shape memory alloys, Advances in Vibration Engineering, Vol. 8, No. 3, pp. 247–254.

He, Y.Y., Oi, S., Chu, F.L. and Li, H.X., 2007a, Vibration control of a rotor-bearing system using shape memory alloy: I. theory, Smart Materials and Structures, Vol. 16, No. 1, pp. 114–121.

He, Y.Y., Oi, S., Chu, F.L. and Li, H.X., 2007b, Vibration control of a rotor-bearing system using shape memory alloy: II. experimental study, Smart Materials and Structures, Vol. 16, No. 1, pp. 122–127.

Inman, D.J., Cartmell, M.P., Lees, A.W., Leize, T. and Atepor, L., 2006, Proposals for controlling flexible rotor vibrations by means of an antagonistic SMA/composite smart bearing, Applied Mechanics and Materials, Vol. 5-6, pp. 29–36.

Janke, L., Czaderski, C., Motavalli, M. and Ruth, J., 2005, Applications of shape memory alloys in civil engineering structures – overview, limits and new ideas, Materials and Structures, Vol. 38, No. 5, pp. 578–592.

Lagoudas, D.C. and Hartl, D.J., 2007, Aerospace applications of shape memory alloys, Proceedings of the Institution of Mechanical Engineers, Part G: Journal of Aerospace Engineering, Vol. 221, No. 4, pp. 535–552.

Lees, A.W., Jana, S., Inman, D.J. and Cartmell, M.P., 2007, The control of bearing stiffness using shape memory, Proceesings of the International Symposium on Stability Control of Rotating Machinery, pp. 299–308.

Liang, C. and Rogers, C.A., 1993, Design of shape memory alloy springs with applications in vibration control, Journal of Vibration and Acoustics, Vol. 115, No. 1, pp. 129–135.

Nagaya, K., Takeda, S., Tsukui, Y. and Kumaido, T., 1987, Active control method for passing through critical speeds of rotating shafts by changing stiffnesses of the supports with use of memory metals, Journal of Sound and Vibration, Vol. 113, No. 2, pp. 307–315.

Nie, J. and Yan, X., 2000, Intelligent bearing system for passing through critical speed of aeroengine rotor by changing stiffness using SMA wires, Materials Science Forum, Vol. 327-328, pp. 99–102.

Żak, A.J., Cartmell, M.P. and Ostachowicz, W.M., 2003, Dynamics and control of a rotor using an integrated SMA/composite active bearing actuator, Key Engineering Materials, Vol. 245-246, pp. 233–240.

RESPONSIBILITY NOTICE

The authors are the only responsible for the printed material included in this paper.